EPR and ENDOR Evidence for a 1-His, Hydroxo-Bridged Mixed-Valent Diiron Site in *Desulfovibrio vulgaris* Rubrerythrin†

Stoyan K. Smoukov,‡ Roman M. Davydov,‡ Peter E. Doan,‡ Bradley Sturgeon,‡ Irene Y. Kung,§ Brian M. Hoffman,‡ and Donald M. Kurtz, Jr.*,§

Department of Chemistry, Northwestern University, Evanston, Illinois 60208, and Department of Chemistry and Center for Metalloenzyme Studies, University of Georgia, Athens, Georgia 30602

Received January 2, 2003

ABSTRACT: Key features differentiating the coordination environment of the two irons in the mixed-valent (Fe^{2+},Fe^{3+}) diiron site of *Desulfovibrio vulgaris* rubrerythrin (Rbr_{mv}) were determined by continuous wave (CW) and pulsed ENDOR spectroscopy at 35GHz. ^{14}N ENDOR evidence indicates that a nitrogen is bound only to the Fe^{2+} ion of the mixed-valent site. Assuming that this nitrogen is from His131Nδ, the same one that furnishes an iron ligand in the crystal structure of the diferric site, the ENDOR data allow us to specify the Fe^{2+} and Fe^{3+} positions within the molecular reference frame. In addition, the $^{1,2}H$ ENDOR on Rbr_{mv} indicates the presence of a solvent-derived aqua/hydroxo ligand bound either terminally or in a bridging mode to Fe^{3+} in the mixed-valent site. The relatively large *g* anisotropy of Rbr_{mv} and weak antiferromagnetic coupling, $J \sim -8$ cm^{-1} (in the $2JS_1 \bullet S_2$ formalism), between the irons is more consistent with a bridging than terminal hydroxo ligand. γ-Irradiation was used to cryoreduce Rbr at 77 K, thereby producing a mixed-valent diiron site [$(Rbr_{ox})_{mv}$] that retains the structure of the diferric site. The EPR spectrum of $(Rbr_{ox})_{mv}$ was nearly identical to that of the as-isolated or chemically reduced samples. This near identity implies that the structure of the mixed-valent Rbr diiron site is essentially identical to that of the diferric site, except for protonation of the oxo bridge, which apparently occurred via a proton jump from hydrogen-bonded solvent at 77 K. The EPR spectrum of $(Rbr_{ox})_{mv}$ thus supports the ^{14}N ENDOR-assigned His131 ligation to Fe^{2+} and assignment of the solvent-derived ligand observed in the $^{1,2}H$ ENDOR to a hydroxo bridge between the irons of the mixed-valent diiron site.

A unique combination of an [$Fe(SCys)_4$] site and a non-sulfur, oxo-bridged diiron site was first described in a protein isolated from the anaerobic sulfate-reducing bacterium, *Desulfovibrio vulgaris* (*1*). The combination of sites in this protein led to the trivial name, rubrerythrin (Rbr),[1] which is a contraction of rubredoxin and hemerythrin (Hr), the prototypical proteins containing these respective sites. Although at least a dozen Rbr homologues or their genes have been subsequently identified from a variety of air-sensitive bacteria and archaea (*2*), the function of Rbr remained unknown until recently. Within the past few years, Rbr has been implicated as one component of a newly described oxidative stress protection system in anaerobic microorganisms (*3*, *4*). Recent evidence, both in vivo (*5*−*7*) and in vitro (*2*, *8*, *9*), indicates that Rbr can function as the terminal component of an NADH peroxidase (reaction 1) and/or a rubredoxin (Rub) peroxidase (reaction 2) in air-sensitive bacteria and archaea.

$$NADH + H^+ + H_2O_2 \rightarrow NAD^+ + 2H_2O \quad (1)$$

$$2H^+ + 2Rub_{red} + H_2O_2 \rightarrow 2Rub_{ox} + 2H_2O \quad (2)$$

In catalyzing reactions 1 and 2, the diferrous site of fully reduced (all-ferrous) Rbr (Rbr_{red}) appears to directly reduce H_2O_2, while the [$Fe(SCys)_4$] site funnels electrons from the exogenous donors to the diiron site (*2*).

In contrast to its rapid (millisecond time scale) reaction with H_2O_2, the diferrous site of Rbr has been found to be only sluggishly reactive (several minutes) with O_2 (*2*, *3*, *8*). This relative sluggishness is somewhat surprising because the diiron-ligating sequence motif and structure of Rbr (*10*) are both homologous to those in a class of enzymes where the diiron sites are known to rapidly (millisecond time scale) activate O_2 for oxidation of another substrate (*11*, *12*). The most thoroughly studied of these O_2-activating enzymes are ribonucleotide reductase R2 subunit (RNR-R2) and the hydroxylase component of methane monooxygenase (MMOH) (*13*, *14*). The X-ray crystal structure of oxidized (all-ferric) *D. vulgaris* Rbr (*10*) indicated that one source of the

† This work was supported by grants from the National Institutes of Health (HL13531 to B.M.H. and GM40388 to D.M.K.).

* To whom correspondence should be addressed. Phone: (706) 542-2016. Fax: (706) 542-9454. E-mail: kurtz@chem.uga.edu.

‡ Northwestern University.

§ University of Georgia.

[1] Abbreviations: Rbr, rubrerythrin; Rbr_{ox}, Rbr containing diferric diiron sites and ferric [$Fe(SCys)_4$] sites; Rbr_{mv}, Rbr containing mixed-valent (Fe^{2+}, Fe^{3+}) diiron and ferric [$Fe(SCys)_4$] sites; Rbr_{red}, all-ferrous Rbr; $(Rbr_{ox})_{mv}$, Rbr_{ox} after cryoreduction to produce additional mixed-valent (Fe^{2+}, Fe^{3+}) diiron sites; Hr, hemerythrin; NADH, reduced nicotinamide adenine dinucleotide; MMOH, methane monooxygenase hydroxylase; RNR R2, ribonucleotide reductase R2 protein; PAP, purple acid phosphatase; Uf, uteroferrin; EPR, electron paramagnetic resonance; ENDOR, electron nuclear double resonance; CW, continuous wave; Hepes, 4-(2-hydroxyethyl)-1-piperazineethanesulfonate.

10.1021/bi0300027 CCC: $25.00
Published on Web 04/30/2003

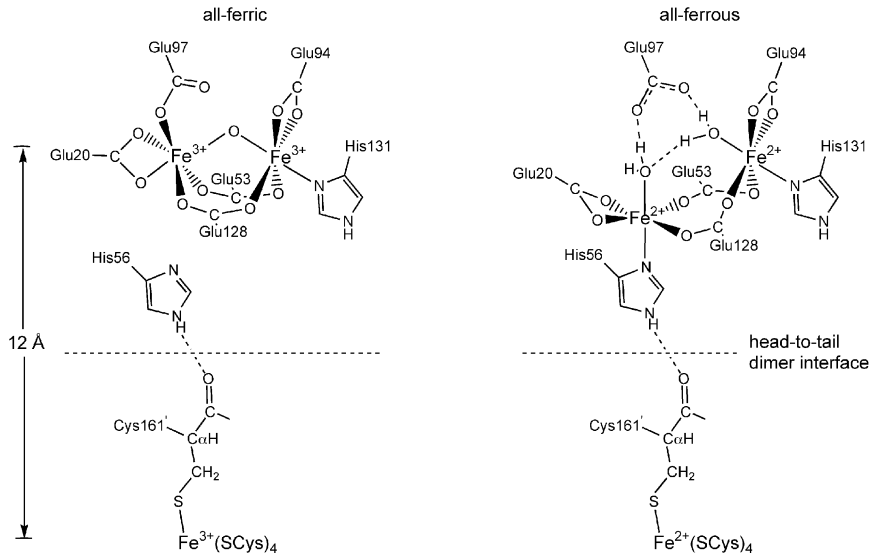

FIGURE 1: Schematic structures of the diferric and diferrous sites in *D. vulgaris* Rbr (top) showing their proximity to the $[Fe(SCys)_4]$ site (bottom) across the subunit interface of the head-to-tail dimer (*10*, *17*).

difference in reactivity may lie in an unanticipated, and so far unique, ligation feature of the diiron site, which is shown in Figure 1. The diiron coordination sphere in the O_2-activating enzymes typically includes six protein ligands, consisting of four carboxylates (from Asp or Glu) and two histidyl imidazoles (*11*). On the basis of this characteristic diiron-ligating sequence motif, both His131 and His56 in *D. vulgaris* Rbr (residues that are conserved in all known Rbrs) had been predicted to furnish ligands to the diiron site (*15*). However, the crystal structure of the diferric site in *D. vulgaris* Rbr showed that while His 131Nδ is indeed a ligand, the Nδ of His56 is 4.2 Å away (and His56Nϵ is even farther) from the nearest iron (i.e., too far away to be a ligand). Instead, Glu97 provides an unexpected carboxylate ligand (Fe−Oϵ1Glu distance of 2.1 Å) that is approximately trans to the His56 nonligand. The His56NϵH is hydrogen-bonded to the carbonyl of a cysteine ligand to the $[Fe(SCys)_4]$ site across the subunit interface of the dimer, which is the presumed route of electron transfer between the two iron sites over a distance of ∼12 Å (cf. Figure 1). Redox-induced His56 ↔ Glu97 ligand switching at the diiron site was suggested, based on the crystal structure of a Glu97Ala Rbr variant (*16*) and on Lewis acidity considerations (*2*). The recently reported X-ray crystal structure of the all-ferrous *D. vulgaris* Rbr (*17*) proved that the proposed His56 ↔ Glu97 ligand switching does indeed occur, as shown schematically in Figure 1. In addition to the terminal ligand substitution of Glu97 by His56 upon reduction, the oxo bridge between the irons of the diferric site is replaced in the diferrous site by two terminal solvent ligands, whereas the carboxylate bridges are retained. The structure of the mixed-valent diiron site in Rbr, which could also be functionally relevant during peroxidase turnover, is not known and may be difficult to determine crystallographically since it tends to partially disproportionate (*18*). Given the structural interconversion diagrammed in Figure 1, the structure of the mixed-valent diiron site could in principle more closely resemble that of either the diferric or diferrous sites.[2]

The mixed-valent (Fe^{3+}, Fe^{2+}) states of carboxylate-bridged diiron sites in proteins typically give rise to axial or rhombic $S = 1/2$ EPR signals with $g_{ave} < 2$ because of weak antiferromagnetic coupling ($-J$ in the range of 6−30 cm^{-1} expressed in the $-2JS_1 \bullet S_2$ formalism) between the irons (*22*−*26*). Such an EPR signal is also observed for as-isolated Rbr (*1*) and was one of the original evidences for a diiron site, although the strength of the antiferromagnetic coupling between the irons has not been reported. ENDOR has proven to be an insightful probe of these mixed-valent sites. For example, ENDOR identified proton signals from bridging hydroxo ligands in the mixed-valent diiron sites of hemerythrin, MMOH, and Uf, as well as the proton signal from a terminal solvent in the latter two proteins (*26*−*28*). ENDOR also identified ^{14}N signals of the ligating histidines in these enzymes. In this paper, we describe EPR and ENDOR studies of the mixed-valent (Fe^{3+}, Fe^{2+}) diiron site of *D. vulgaris* Rbr, the results of which provide unprecedented insights into its coordination sphere, particularly regarding the histidine ligands and solvent, and its electronic structure. Given the aforementioned difficulty in obtaining crystalline Rbr that reliably contains a mixed-valent diiron site, the ENDOR studies reported here represent an important alternative approach to obtaining structural and electronic information about this unique member of the non-heme, non-sulfur class of diiron enzymes.

MATERIALS AND METHODS

Recombinant *D. vulgaris* Rbr was prepared and quantitated as described previously (*18*). To enhance the proportion of mixed-valent diiron sites, the as-isolated Rbr (0.7−1 mM in diiron sites) in 50 mM Hepes and 200 mM sodium sulfate (pH 7.0) was treated with approximately equimolar dithiothreitol and allowed to react anaerobically for approximately

[2] A considerable body of evidence (*1*, *3*, *19*) indicates that the recently reported Zn, Fe rather than diiron site in *D. vulgaris* Rbr (*20*, *21*) is an artifact of isolation and/or crystallization.

1 h at room temperature before transferring 60-μL aliquots to ENDOR sample tubes and freezing in a liquid N_2 bath. Rbr samples in D_2O were prepared identically after repeated concentrations and dilutions of Rbr with the Hepes buffer listed above that had been prepared in D_2O.

X-band EPR spectra were recorded as previously described (*18*). An estimate of the antiferromagnetic coupling between the irons of the mixed-valent Rbr diiron site was determined from the temperature dependence of the half-saturation powers of the EPR signal intensities at $g = 1.76$ and assuming an Orbach process, as previously described for other $S = 1/2$-ground state, mixed-valent diiron sites in proteins (*23*, *24*).

Previously described 35 GHz CW (*29*) and pulsed ENDOR instrumentation (*30*) and procedures were applied. Spectra were recorded at 2 K. The magnet power supply on the 35 GHz pulsed ENDOR instrument permitted us to collect data up to fields of ~16 500 G, corresponding to $g \sim 1.52$, thus covering the entire Rbr EPR envelope. The power supply of our CW ENDOR instrument restricts us to fields less than 14 500 G, corresponding to $g \sim 1.72$. The Mims three-pulse (*31*, *32*), Re-Mims four-pulse (*33*), and the Davies (*34*) three-pulse techniques were used to collect pulsed ENDOR spectra.

The Mims technique utilizes a three pulse electron spin−echo sequence ($t_p - \tau - t_p - T - t_p - \tau -$ echo), where t_p is the microwave pulse width, and the R_f pulse is inserted during the interval, T (*31*, *32*). For a nucleus with hyperfine coupling, A, this technique has a response R that depends on the product, $A\tau$, according to the equation $R \sim [1 - \cos(2\pi A\tau)]$. This function has zeroes, corresponding to minima in the ENDOR response (hyperfine suppression holes) at $A\tau = n$ and maxima at $A\tau = (2n + 1)/2$; $n = 0, 1, ...$ The shortest τ value achievable in a Mims sequence on our 35 GHz pulsed spectrometer is 300−350 ns. The Re-Mims four-pulse (*34*) ENDOR technique permits the use of much shorter values of τ and was applied as needed. This technique also displays the suppression holes characteristic of the Mims sequence but makes the choice of τ independent of deadtime. The Davies technique signal intensity depends not on the product, $A\tau$, but on the product, At_p (*35*), and is most useful for nuclei with large hyperfine couplings.

The ENDOR pattern for a single molecular orientation from a nucleus with spin I consists of two branches of $2I$ lines each, with first-order frequencies $\nu \pm^{(m)} = |\nu_N \pm A/2 + 3/2P(2m - 1)|$, $I \geq m \geq -I + 1$, where A and P are the orientation-dependent hyperfine and quadrupole couplings. All ENDOR signals displayed here, except those for ^{14}N, arise from nuclei with Larmor frequencies $\nu > A/2$, in which case the two branches are centered at the Larmor frequency and separated by the hyperfine interaction, A. The ^{14}N signals, with $A/2 < \nu$, are centered at $A/2$, and the two branches are separated by twice the ^{14}N Larmor frequency. Techniques for simulating frozen-solution spectra and for analyzing 2-D field-frequency plots comprised of multiple ENDOR spectra taken across the EPR envelope of a paramagnetic center in a frozen solution have been published (*36*, *37*).

Investigation of the EPR-silent diferric (oxidized) site structure of Rbr (Rbr_{ox}) was made possible through the use of samples of the as-isolated Rbr that had been radiolytically cryoreduced by γ-irradiation at 77 K (*38*). This technique produces an EPR-active mixed-valence state, denoted $(Rbr_{ox})_{mv}$, frozen in the original geometry of the diferric site.

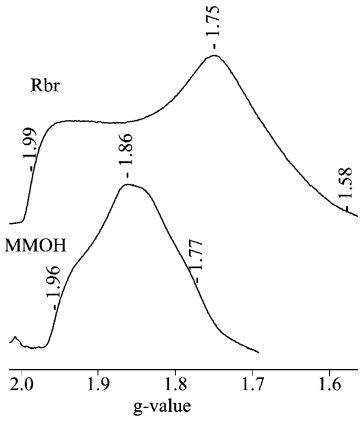

FIGURE 2: EPR spectra, presented in absorption mode, of *D. vulgaris* Rbr_{mv} (top) and *M. capsulatus* $MMOH_{mv}$ (bottom) both obtained at 2 K. Other conditions were, for Rbr: three-pulse echo-detected EPR at 34.816 GHz, $t_p = 52$ ns, $T = 73.38$ μs, $\tau = 480$ ns, 96 data shots/point acquired at a 10-ms repetition rate, and 500-s scan and for MMOH: CW at 35.155 GHz, 2 G modulation amplitude, 8-min scan, 64-ms time constant.

RESULTS

Comparison of Rbr_{mv} versus $MMOH_{mv}$ EPR. The diiron site of as-isolated Rbr is primarily in the EPR-silent Rbr_{ox} diferric state, with a minor portion (<25%) in the mixed-valent, (Rbr_{mv}) state (*18*). The **g** tensor of the diiron site in Rbr_{mv}, **g** = [1.99, 1.75, 1.58], has been reported previously from X-band EPR spectra (*1*), and chemical reduction with DTT increases the strength of this signal without changing its shape. The diiron sites in the as-isolated and chemically reduced forms of Rbr_{mv} are thus indistinguishable by EPR. Figure 2, showing Q-band absorption-mode EPR spectra, illustrates the larger g anisotropy of Rbr_{mv} as compared to that of $MMOH_{mv}$, whose mixed-valent diiron site has been shown to have a hydroxo bridge between the two iron atoms (*27*, *39*). For such mixed-valent sites, the hydroxo bridge is the major source of superexchange antiferromagnetic coupling that gives rise to the $S = 1/2$ ground state. An estimate of the strength of antiferromagnetic coupling between the irons in Rbr_{rmv} was obtained from the power saturation behavior of the X-band EPR spectrum as a function of temperature. For an Orbach relaxation process, this analysis gives an estimate of the energy separation between the ground $S = 1/2$ and first excited $S = 3/2$ spin states, which is equivalent to $-3J$ in the $-2JS_1 \bullet S_2$ formalism (*23*). From this analysis (cf. Figure S2 in Supporting Information), J is estimated to be -8 cm^{-1} in Rbr_{mv}. A similar analysis gave J of -30 cm^{-1} for the MMOH mixed-valent diiron site (*24*). For reasons elaborated in the Discussion, relatively large g anisotropies and $-J$ values of 8 and 30 cm^{-1} are associated with hydroxo rather than oxo bridges in mixed-valent, non-heme diiron complexes and proteins.

^{14}N ENDOR of Rbr_{mv}. Figure 3 compares the ^{14}N ENDOR spectra of $MMOH_{mv}$ and Rbr_{mv}. Previous studies (*27*) established that the ^{14}N ENDOR spectrum of $MMOH_{mv}$ exhibits signals for two histidyl nitrogens, one bound to the ferrous and one to the ferric ion. The peaks in the 2−8 MHz region for $MMOH_{mv}$ are assignable to ν^+ of histidine ^{14}N bound to Fe^{2+}; peaks in the region of 10−15 MHz, which are also much more intense, are assignable to ν^+ of ^{14}N bound to the Fe^{3+}.

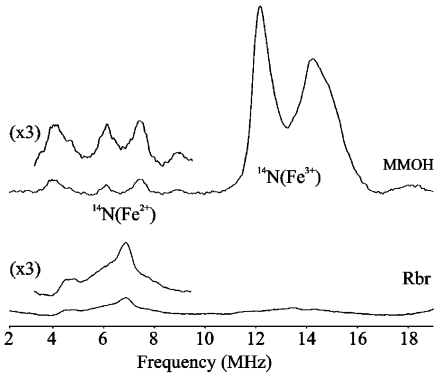

FIGURE 3: ^{14}N CW ENDOR of *M. capsulatus* $MMOH_{mv}$ (top; from ref *27*) and *D. vulgaris* Rbr_{mv} (bottom) both obtained at 2 K. Other conditions were, for $MMOH_{mv}$: 35.0 GHz, modulation amplitude = 0.3 G and for Rbr_{mv}: 34.9 GHz, modulation amplitude = 0.6 G, g = 1.75, 50 scans, and sweep rate = 1 MHz/s.

The ^{14}N ENDOR study of $MMOH_{mv}$ further shows that the hyperfine tensor of a histidyl nitrogen bound to either the ferric or ferrous ion of a mixed-valence diiron center is almost isotropic, $\mathbf{a}^{3+}(^{14}N) \sim 25$ MHz; $\mathbf{a}^{2+}(^{14}N) \sim 7$ MHz (*27*); hence, the simple comparison of the two proteins at the single field is adequate for our purposes. The difference in the observed ^{14}N hyperfine coupling, and thus ENDOR frequencies (see Materials and Methods), for the ^{14}N bound to Fe^{3+} and Fe^{2+} in a diiron center is largely the consequence of the spin coupling between the two Fe ions: the observed hyperfine tensor, $\mathbf{A}^{n+}(^{14}N)$, for a ^{14}N ligand to an Fe^{n+} ion (n = 2 or 3) in a spin-coupled diiron center is related to the intrinsic coupling, $\mathbf{a}^{n+}(^{14}N)$, as $\mathbf{A}^{3+}(^{14}N) \sim (7/3)\ \mathbf{a}^{3+}(^{14}N)$ and $\mathbf{A}^{2+}(^{14}N) \sim -(4/3)\ \mathbf{a}^{2+}(^{14}N)$ (*27*). Analysis of the observed hyperfine couplings in this way shows that the intrinsic ^{14}N couplings for the histidyl nitrogen bound to the two iron ions are not greatly different, even though their observed couplings are strongly different.

In contrast to $MMOH_{mv}$, the corresponding spectrum of Rbr_{mv} (Figure 3) shows peaks only from a single ^{14}N, with $\mathbf{A}(^{14}N) \sim 6$ MHz. By comparison with the couplings for the two histidyl ligands in $MMOH_{mv}$, this small coupling must be assigned to a His bound to the ferrous ion of the mixed-valence center. The crystal structure of the diferric form of Rbr (cf. Figure 1) (*10*) shows that the Nδ nitrogen of His131 is coordinated to one iron, while the second proximal histidine (His56) is not coordinated to either iron. The straightforward conclusion from our ^{14}N ENDOR measurements is that reduction to Rbr_{mv} occurs without change in ligation of the diiron site and that His131 is coordinated to the Fe^{2+} ion of the mixed-valent Rbr diiron site, while His56 remains unbound.

^{1,2}H ENDOR of Rbr_{mv}. ^{1}H ENDOR spectra of Rbr_{mv} taken at g_1 and other fields between g_1 and g_2 revealed a strongly coupled proton ($A_{max} \sim 25$ MHz), which is not present in a sample exchanged into D_2O (cf. Figure 4). Our previous studies show that such a strongly coupled, exchangeable proton signal can come only from a water/hydroxide bound to the Fe^{3+}, either terminally or as a bridge to another metal ion (*27*, *28*, *40*). An interesting feature of these spectra is that the ν^- and ν^+ peaks of the strongly coupled proton are inverted, a spin relaxation phenomenon that is observed occasionally (*36*) (and in some cases partially understood (*41*)).

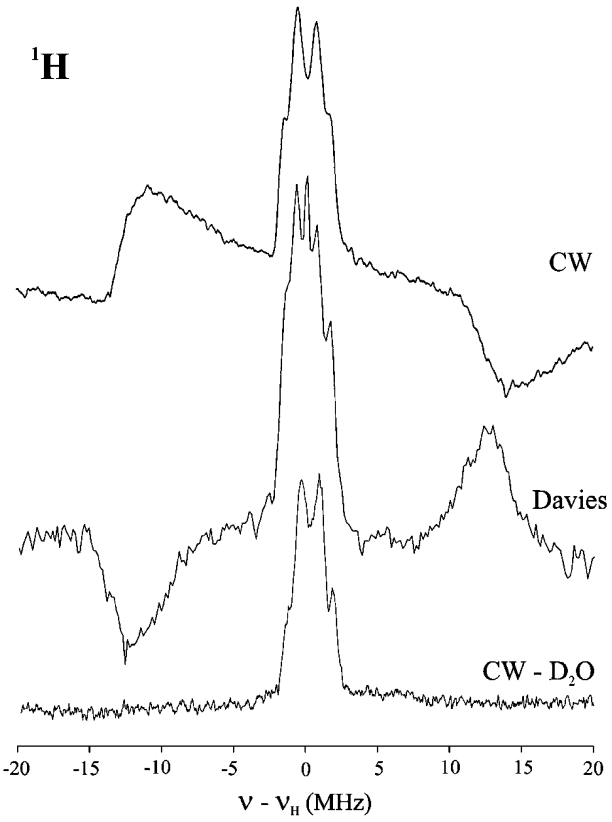

FIGURE 4: ENDOR of Rbr_{mv} at g_1. Conditions were, for CW: 2 K; 35.1 GHz; modulation amplitude = 2 G; sweep rate = 3 MHz/s; for Davies pulsed: 2 K, g = 1.974, 34.816 GHz; τ = 480ns; $t_{\pi/2}$ = 76 ns; R_f word = 100 μs; repetition time = 10 ms; scans = 2; for CW, sample exchanged in D_2O: 2 K; 35.1 GHz; modulation amplitude = 2 G; sweep rate = 1 MHz/s.

Bridging and terminal solvent ligands can often be distinguished from each other by their 2-D field-frequency ENDOR spectral patterns (*26*, *27*, *40*). CW ^{1}H ENDOR spectra of Rbr_{mv} gave a 2-D field-frequency pattern (cf. Figure S1 in Supporting Information) in which the hyperfine coupling was largest at g_1 and then quickly decreased as the field was increased from g_1 toward g_2. For a variety of reasons, including the cutoff of our magnet, useful CW spectra could be collected only for $g \geq 1.86$. To obtain a complete 2-D data set, we employed ^{2}H pulsed ENDOR at 35 GHz on a sample of Rbr_{mv} in D_2O (cf. Figure 5). These spectra followed the same pattern between g_1 and g_2 as seen in the CW spectra (cf. Figure S1) but cover the full EPR envelope.

Simulations of the 2-D field-frequency pattern of the ^{1,2}H ENDOR spectra were performed in an effort to determine whether the solvent-derived Fe^{3+} ligand was terminally ligated or bridging to Fe^{2+}. The simulations employed a model in which the dipolar interactions with the two Fe ions are summed analytically, as described previously (*27*, *40*). Both the bridging and terminal simulations yielded hyperfine tensors that gave acceptable matches to the data in Figure 5. The inability of the simulations to distinguish between bridging and terminal ligation was due in part to the broad peaks and low signal-to-noise ratio, especially near g_3, but some features inherent to the analysis also make this discrimination difficult (cf. Discussion). Nevertheless, the hyperfine tensors derived from the simulations are consistent

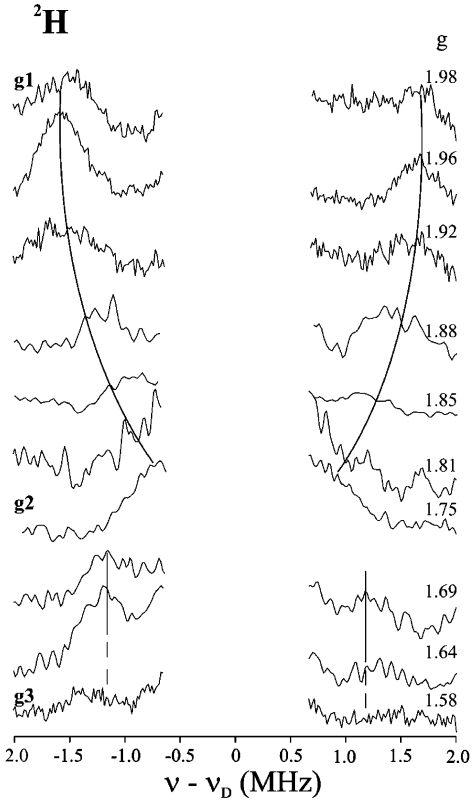

FIGURE 5: ^{2}H pulsed ENDOR spectra of Rbr_{mv} exchanged in D_2O. Spectra are identified by their *g* values. Conditions for the various *g* values were 1.98, 34.60 GHz, Mims pulse sequence with $\pi/2$ microwave pulse $t_p = 52$ ns, 60 μs R_f pulse, $\tau = 480$ ns, repetition time = 15 ms, 60 averaged data shots per point; 10 scans; 1.96: same as for 1.98 except 5 scans; 1.92, same as 1.98; 1.88, same as 1.98 except 34.63 GHz, $\tau = 536$ ns, repetition time = 10 ms; 1.85, same as 1.88 except $\tau = 676$ ns, 30 scans; 1.81, 34.64 GHz, Re-Mims pulse sequence with $\pi/2$ microwave pulse = 32 ns, 60 μs R_f pulse, $\tau = 180$ ns, repetition time = 20 ms, 50 averaged data shots per point; 10 scans; 1.75 and 1.69, same as 1.81; 1.64, same as 1.81 except 40 scans; 1.58, same as 1.98 except 14 scans.

with assignment to a bridging hydroxo ligand, in agreement with the EPR **g** tensor anisotropy. The simulation that placed the protons on a terminal aqua/hydoxo ligand required inclusion of a substantial isotropic hyperfine component in the hyperfine tensor $\mathbf{A}(^2H) = [3.25, -2.5, -2.5]$ MHz, with isotropic component $\mathbf{a}_{iso}(^2H) = -0.58$ MHz, (corresponding to $\mathbf{a}_{iso}(^1H) = -3.8$ MHz). No such isotropic component has been found in previous studies of a terminally bound solvent ligand to Fe^{3+} (*40*). In contrast, the dipolar hyperfine tensor derived for the hydroxo bridge in MMOH, $\mathbf{A}(^2H) = [-3.84, -0.77, 4.60]$ MHz, $\mathbf{a}_{iso}(^2H) = 0$ (*27*), could be used directly with minimal change, namely, a different orientation with respect to the **g** tensor and a reduction in the individual hyperfine couplings by 20%. The smaller ^{1,2}H hyperfine couplings may reflect slightly longer Fe−OH bridge bond distances in Rbr_{mv} than in MMOH or the effects of the zero-field splittings on the individual Fe^{2+} and Fe^{3+} ions in altering the observed hyperfine couplings.[3] These findings argue against the assignment of this proton signal as a terminal aqua/hydroxo ligand and support its assignment to a hydroxo bridge.[4]

[3] Smoukov, S., and Hoffman, B. M., to be published.

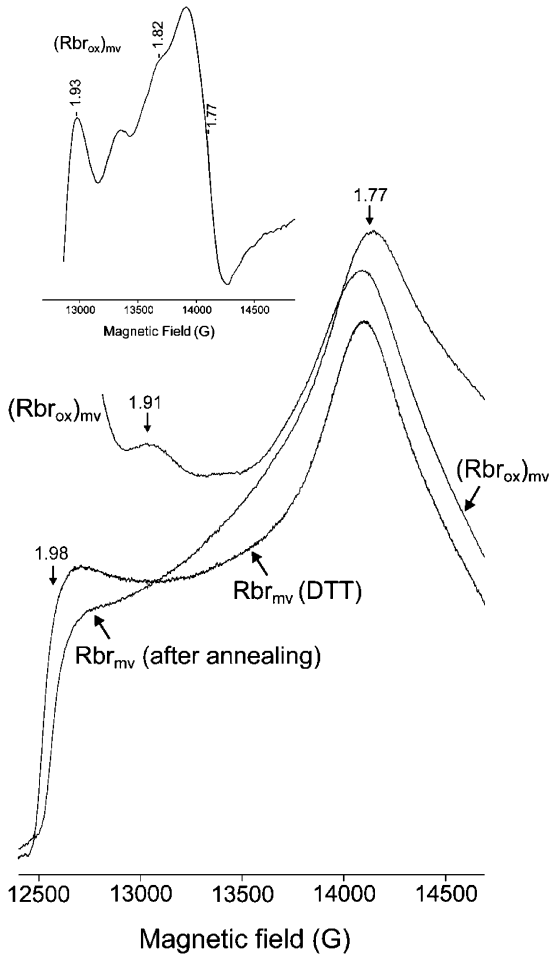

FIGURE 6: EPR spectra, presented in absorption mode, of $(Rbr_{ox})_{mv}$ and Rbr_{mv}, both after annealing of $(Rbr_{ox})_{mv}$ (after annealing) and chemically produced by reduction of Rbr_{ox} with dithiothreitol (DTT). Spectral conditions were, for $(Rbr_{ox})_{mv}$: 34.926 GHz, 2 K, modulation amplitude = 5 G, MW power = 30 dB; for Rbr_{mv} (after annealing): 34.945 GHz, 2 K, modulation amplitude = 5 G, MW power = 30 dB; for Rbr_{mv} (DTT): 34.909 GHz, 2 K, modulation amplitude = 2 G; MW power = 30 dB. Inset shows $(Rbr_{ox})_{mv}$ EPR spectrum in first derivative mode.

Cryoreduction of Rbr$_{ox}$. Low temperature (77 K) cryoreduction (*38*) of as-isolated Rbr yielded a mixed-valent form trapped in the structure of the Rbr_{ox} precursor; we refer to this state as $(Rbr_{ox})_{mv}$. The EPR signal of this $(Rbr_{ox})_{mv}$, shown in Figure 6, is essentially identical in shape but approximately 2-fold more intense than the signal from the [Fe^{2+}, Fe^{3+}] site that was already present in the as-isolated Rbr. This signal does not change upon annealing the cryoreduced sample to room temperature. Since the only possible source of the increase in Rbr_{mv} signal intensity is cryoreduction of Rbr_{ox} (reduction of the preexisting Rbr_{mv} form would yield the EPR-silent diferrous state), the EPR signals of Rbr_{mv} and $(Rbr_{ox})_{mv}$ must be essentially identical to each other. This identity in turn implies that $(Rbr_{ox})_{mv}$ and thus Rbr_{ox} have essentially the same ligand set and overall coordination geometry as that of the chemically produced Rbr_{mv}. Therefore, since the diferric center in Rbr_{ox} does not

[4] We cannot be more definitive about this assignment because our analysis of 2-D ENDOR spectra of diiron sites involves diagonalization of the sum of the hyperfine interactions of a proton with the two iron ions to yield a single fictitious hyperfine tensor. This approach becomes less satisfactory when the *g* anisotropy becomes large.

Scheme 1

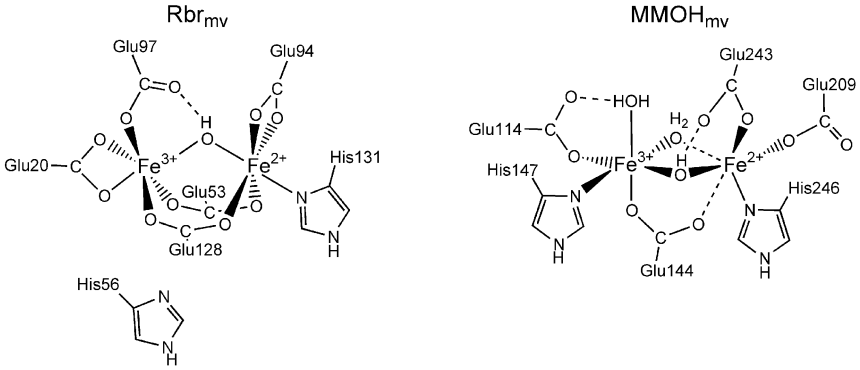

have His56 as a ligand, (cf. Figure 1) (*10*), neither must the mixed-valent diiron site. Our cryoreduction results thus support our ^{14}N ENDOR results, showing that the diiron center of Rbr$_{mv}$ has only one His ligand.

Rbr$_{ox}$ apparently differs from Rbr$_{mv}$ and (Rbr$_{ox}$)$_{mv}$ in one significant respect, however: Rbr$_{ox}$ has an oxo bridge (*10*, *19*), while the ^{1,2}H ENDOR data are interpreted to indicate that Rbr$_{mv}$, and because of its identical EPR signal, (Rbr$_{ox}$)$_{mv}$ too, have a hydroxo bridge. If so, then the (Rbr$_{ox}$)$_{mv}$ we observe upon 77 K cryoreduction cannot be the primary reduction product but must rather be the result of a subsequent low-barrier proton jump from proximal solvent to the oxo bridge at 77 K. The EPR of the cryoreduced sample also contains a trace signal from a species with a feature at $g = 1.93$ that is lost during annealing (cf. Figure 6). We provisionally assign this trace signal as the primary product of cryoreduction (i.e., to an oxo-bridged mixed-valent diiron site that forms prior to the proton jump).

DISCUSSION

Our ^{14}N ENDOR data show that the diiron site of Rbr$_{mv}$ has a single His ligand to the ferrous ion, and the ^{1,2}H ENDOR supports the presence of a hydroxo bridge between the irons that, for reasons discussed below, is inferred from both the large EPR g anisotropy and the J value of -8 cm^{-1} of Rbr$_{mv}$. The cryoreduction EPR experiments complement the ^{14}N ENDOR data in indicating that, with the exception of the oxo/hydroxo bridge change, there is no difference in the ligand set and overall coordination geometries of Rbr$_{ox}$ and Rbr$_{mv}$. The straightforward interpretation of our EPR/ENDOR results is summarized in the proposed Rbr$_{mv}$ diiron site structure shown in Scheme 1.

The proposed Rbr$_{mv}$ diiron site structure in Scheme 1, when compared with that of the diferric site shown in Figure 1, indicates very little structural rearrangement upon reduction to the mixed-valent level, other than protonation of the oxo bridge. We thus propose that the His131-bound iron seen in the crystal structure of the diferric site in Rbr$_{ox}$ (*10*) is ultimately reduced upon formation of the [Fe^{2+}, Fe^{3+}] site in Rbr$_{mv}$, while the proximal His56 remains unbound. This conclusion agrees with the expectation that the iron ligated to the charge-neutral His131 side chain rather than the anionic Glu97 carboxylate would stabilize Fe^{2+} relative to Fe^{3+} in the mixed-valent site. This situation is reminiscent of the mixed-valent, spin-coupled [2Fe$-$2S]$^{+}$ Rieske center, in which two anionic cysteine thiolate sulfurs are coordinated to the Fe^{3+}, and two neutral histidine Nδ nitrogens are coordinated to the Fe^{2+} (*42*).

This report also constitutes the first ENDOR assignment of the Fe^{2+} and Fe^{3+} ions of a mixed-valent carboxylate-bridged center in the molecular frame of reference. The only other such assignment for a diiron carboxylate protein was recently reported for MMOH$_{mv}$ on the basis of bond distances in the crystal structure (*39*). This MMOH$_{mv}$ mixed-valent diiron site structure is shown for comparison in Scheme 1. In certain cases of asymmetrically ligated diiron sites or via residue-specific isotope labeling of ligands, ENDOR may prove to be a powerful complement to X-ray crystallography in metal oxidation state determinations, especially when the oxidation state of interest is too ephemeral to be trapped quantitatively in a crystal.

As shown in Scheme 1, we favor assignment of the exchangeable ^{1}H ENDOR signal from Rbr$_{mv}$ (cf. Figures 4 and 5) to a bridging hydroxo ligand. The analysis of strongly coupled ($A_{max} > \sim$8 MHz) ^{1}H ENDOR signals from water-derived ligands to mixed-valent diiron centers started with the characterization of the signal from the hydroxo bridges of Hr$_{mv}$ and MMOH$_{mv}$, which show similar behavior (*28*). In both cases the **A** tensor is highly rhombic (**A** $\sim$[30, -5, -25]), and the orientation of **g** relative to the molecular frame, and thus of **A** relative to **g**, can vary (*26*). The maximum ^{1}H hyperfine couplings for a hydroxo bridge and a terminal solvent-derived ligand to Fe^{3+} are of the same magnitude, but a terminal solvent ligand typically gives a roughly axial dipolar tensor, $\mathbf{A}^{term} \sim[-T, -T, 2T]$, $2T \sim$25 MHz. Therefore, the only current means of distinguishing between these two classes of protons requires determination of full hyperfine tensors (*27*, *40*).

EPR-active metal sites in proteins often show intense weakly coupled ENDOR signals from more distant protons. Such signals obscure the strongly coupled dipolar proton pattern signals at orientations where the hyperfine couplings are small, making the full tensor determination difficult. In the case of mixed-valent [Fe^{4+}, Fe^{3+}] RNR R2 intermediate X, all the proton/deuteron ENDOR signals arose only from the strongly coupled exchangeable protons/deuterons. Such a background-free pattern allowed the subtle distinction of **A** tensors between the terminal solvent-derived ligand and the hydroxo bridge models and the identification the solvent-derived ligand in RNR R2 intermediate X as a terminal water on Fe^{3+} (*40*). In the case of Uf (the mixed-valent [Fe^{2+}, Fe^{3+}], as-isolated active state) other exchangeable proton signals were present, but a favorable relative orientation of the **A** and **g** tensors was found to be incompatible with the tensor for a terminal water on the Fe^{3+} (*26*).

For Rbr_{mv}, assignment of the ^1H ENDOR signal to a bridging versus terminal solvent ligand is somewhat ambiguous, but several observations favor a bridging hydroxide. First, simulation as a bridging hydroxo required fewer assumptions to fit the ENDOR data. Second, a hydroxo bridge is favored by the relatively large EPR *g* anisotropy. In a study of several synthetic mixed-valent [Fe^{3+}, Fe^{2+}] complexes with single oxygen atom bridges (oxo, hydroxo, phenoxo, or alkoxo), the value of g_3 (the lowest *g* value) was found to be >1.90 for oxo-bridged complexes, <1.80 for hydroxo- (or phenoxo, alkoxo)-bridged complexes, and $=1.85$ for a complex with both kinds of bridges (*43*−*46*). The much larger *g* anisotropy for hydroxo- versus oxo-bridged complexes is consistent with the expression for the **g** tensor anisotropy (*47*). This expression includes a summation term proportional to $D_{Fe^{2+}}/J$, which becomes large for small values of *J*. (*D* is the axial crystal-field-induced ground-state zero-field splitting parameter for the individual ions, and *J* is the antiferromagnetic exchange-coupling term whose magnitude determines the spacing between the ground state $S = 1/2$ spin of the mixed-valent ($S = 5/2$ and $S = 2$) diiron cluster and its higher-spin excited states.) *J* values for mixed-valent, hydroxo-bridged diiron complexes are in the range of 6−30 cm^{-1} versus 80−160 cm^{-1} for oxo-bridged diiron complexes (*43*, *45*, *46*, *48*). $D_{Fe^{2+}}$ is not expected to change so drastically since only small changes in the coordination sphere geometry occur upon interconversion between oxo and hydroxo bridges. The *g* anisotropies should, therefore, be larger for hydroxo- versus oxo-bridged [Fe^{3+}, Fe^{2+}] complexes, and Rbr_{mv} with $g_3 = 1.58$ certainly falls into this category. The *J* value determined for the mixed-valent Rbr diiron site in this work, -8 cm^{-1}, also rules out an oxo bridge and falls near the lower end of the hydroxo-bridged range. Finally, protonation of the oxo bridge upon one-electron reduction of the diferric site would be favored over addition of a terminal water or hydroxide to an oxo-bridged mixed-valent complex on the bases of both charge compensation and minimal structural rearrangements required by the cryoreduction results.

The cryoreduction results, implying no significant structural rearrangement between the Rbr_{ox} and Rbr_{mv} diiron sites, also argue against the possibility that the Rbr_{mv} diiron site has lost the single atom bridge and contains only the two μ-1,3-carboxylato ligands from Glu53 and Glu128 and a terminal solvent ligand to Fe^{3+}. While solely carboxylato-bridged diferrous sites in proteins, including Rbr, are known (*11*, *14*, *17*), we have found no reports of diferric or mixed-valent diiron sites bridged solely by carboxylates, either in proteins or synthetic complexes. Bis(μ-carboxylato)diferrous complexes show only very weak magnetic couplings between the $S = 2$ irons, much smaller than for comparable complexes containing an additional hydroxo bridge; the latter have *J* values similar to those for the corresponding mixed-valent, hydroxo-bridged diiron complexes discussed above (*14*).

The apparent protonation of the oxo bridge upon cryoreduction of Rbr_{ox} at 77 K has not been observed in non-heme diiron sites of other proteins without annealing to higher temperatures (*43*). In this respect, the behavior of the $(Rbr_{ox})_{mv}$ diiron site is more reminiscent of the hydroxo-bridged diferric site of MMOH, whose cryo-produced mixed-valent EPR signal does not change upon annealing (*44*). Nevertheless, resonance Raman spectroscopy of as-isolated *D. vulgaris* Rbr_{ox} at 77 K clearly shows the presence of an oxo bridge (*19*). On the other hand, both the X-ray crystal structure (*10*) and the resonance Raman spectroscopy indicate that solvent hydrogen bonds to the oxo bridge in the diferric site of Rbr_{ox}, perhaps facilitating a proton jump upon cryoreduction. The proposed hydrogen bond between the hydroxo bridge and the Glu97 carboxylate in Rbr_{mv} (cf. Scheme 1) might also lower the energy barrier for this proton jump. A proton jump from solvent to iron-coordinated dioxygen has been observed upon cryoreduction at 77 K of oxy-ferrous heme oxygenase and oxy-ferrous-cytochrome P450, leading directly to the hydroperoxo-ferric species (*49*, *50*).

Both the diferric/mixed-valent and the mixed-valent/diferrous reduction potentials of Rbr are 100−200-mV higher than those of the diiron site in MMOH (*18*). The relatively different coordination spheres for the two irons in the both diferric and mixed-valent forms of the Rbr diiron site (i.e., only one iron containing a His ligand vs both irons in MMOH (cf. Scheme 1)) may contribute to the relative stabilization of the mixed-valent oxidation level in Rbr. The higher mixed-valent/diferrous reduction potential of Rbr could then be due in part to the Glu97 → His56 ligand substitution upon conversion to the diferrous form (cf. Figure 1). Other differing factors that could affect the relative reduction potentials of the diiron sites include the bridging ligands (cf. Scheme 1), net charges on the sites (zero for MMOH (*39*), vs -1 for Rbr), and solvent accessibility (buried in MMOH vs exposed in Rbr (*17*)).

These results clarify the structure of the mixed-valent diiron site in Rbr, which, as outlined in the introductory paragraphs, may constitute a new class of non-heme peroxidases. Preliminary kinetic studies indicate that the mixed-valent Rbr diiron site is a product of rapid two-electron oxidation of the diferrous site in Rbr_{red} by hydrogen peroxide followed by a slower internal electron transfer from the ferrous [$Fe(SCys)_4$] site to the diferric site across the subunit interface shown in Figure 1 (*17*) (Jin, S., Coulter, E. D., Phillips, R. S., and Kurtz, D. M., Jr., unpublished results).

ACKNOWLEDGMENT

We acknowledge Mr. Clark E. Davoust for excellent technical support and Christopher Colangelo, Xiao-yuan Cui, and Shi Jin for isolating and purifying the Rbr used for these studies.

SUPPORTING INFORMATION AVAILABLE

Figures depicting field-dependent ^1H CW ENDOR spectra and EPR power-saturation temperature dependence of Rbr_{mv}. This material is available free of charge via the Internet at http://pubs.acs.org.

NOTE ADDED AFTER ASAP POSTING

This article was released ASAP on 04/30/03 with 60-mL in line 132 rather than 60-μL. The correct version was posted on 05/02/03.

REFERENCES

1. LeGall, J., Prickril, B. C., Moura, I., Xavier, A. V., Moura, J. J. G., and Huynh, B. M. (1988) *Biochemistry 27*, 1636−1642.

2. Coulter, E. D., Shenvi, N. V., Beharry, Z., Smith, J. J., Prickril, B. C., and Kurtz, D. M., Jr. (2000) *Inorg. Chim. Acta 297*, 231−234.
3. Kurtz, D. M., Jr., and Coulter, E. D. (2001) *Chemtracts, Inorg. Chem. 14*, 407−435.
4. Sztukowska, M., Bugno, M., Potempa, J., Travis, J., and Kurtz, D. M., Jr. (2002) *Mol. Microbiol. 44*, 479−488.
5. Alban, P. S., Popham, D. L., Rippere, K. E., and Krieg, N. R. (1998) *J. Appl. Microbiol. 85*, 875−882.
6. Alban, P. S., and Krieg, N. R. (1998) *Can. J. Microbiol. 44*, 87−91.
7. Lumppio, H. L., Shenvi, N. V., Summers, A. O., Voordouw, G., and Kurtz, D. M., Jr. (2001) *J. Bacteriol. 183*, 101−108.
8. Coulter, E. D., Shenvi, N. V., and Kurtz, D. M., Jr. (1999) *Biochem. Biophys. Res. Commun. 255*, 317−323.
9. Coulter, E. D., and Kurtz, D. M., Jr. (2001) *Arch. Biochem. Biophys. 394*, 76−86.
10. deMaré, F., Kurtz, D. M., Jr., and Nordlund, P. (1996) *Nature Struct. Biol. 3*, 539−546.
11. Kurtz, D. M., Jr. (1997) *J. Biol. Inorg. Chem. 2*, 159−167.
12. Nordlund, P., and Eklund, H. (1995) *Curr. Opin. Struct. Biol. 5*, 758−766.
13. Wallar, B. J., and Lipscomb, J. D. (1996) *Chem. Rev. 96*, 2625−2657.
14. Solomon, E. I., Brunold, T. C., Davis, M. I., Kemsley, J. N., Lee, S.-K., Lehnert, N., Neese, F., Skulan, A. J., Yang, Y.-S., and Zhou, J. (2000) *Chem. Rev. 100*, 235−350.
15. Kurtz, D. M., Jr., and Prickril, B. C. (1991) *Biochem. Biophys. Res. Commun. 181*, 337−341.
16. deMaré, F., Nordlund, P., Gupta, N., Shenvi, N. V., Cui, X., and Kurtz, D. M., Jr. (1997) *Inorg. Chim. Acta 263*, 255−262.
17. Jin, S., Kurtz, D. M., Jr., Liu, Z.-J., Rose, J., and Wang, B.-C. (2002) *J. Am. Chem. Soc. 124*, 9845−55.
18. Gupta, N., Bonomi, F., Kurtz, D. M., Jr., Ravi, N., Wang, D. L., and Huynh, B. H. (1995) *Biochemistry 34*, 3310−3318.
19. Dave, B. C., Czernuszewicz, R. S., Prickril, B. C., and Kurtz, D. M., Jr. (1994) *Biochemistry 33*, 3572−3576.
20. Sieker, L. C., Holmes, M., Le Trong, I., Turley, S., Liu, M.-Y., LeGall, J., and Stenkamp, R. E. (2000) *J. Biol. Inorg. Chem. 5*, 505−513.
21. Li, M., Liu, M.-Y., LeGall, J., Gui, L. L., Liao, J., Jiang, T., Zhang, J.-P., Liang, D.-C., and Chang, W.-R. (2003) *J. Biol. Inorg. Chem. 8*, 149−155.
22. Lauffer, R. B., Antanaitis, B. C., Aisen, P., and Que, L., Jr. (1983) *J. Biol. Chem. 258*, 14212−8.
23. Pearce, L. L., Kurtz, D. M., Jr., Xia, Y. M., and Debrunner, P. G. (1987) *J. Am. Chem. Soc. 109*, 7286−7293.
24. Fox, B. G., Liu, Y., Dege, J. E., and Lipscomb, J. D. (1991) *J. Biol. Chem. 266*, 540−550.
25. McCormick, J. M., Reem, R. C., and Solomon, E. I. (1991) *J. Am. Chem. Soc. 113*, 9066−9079.
26. Smoukov, S. K., Quaroni, L., Wang, X., Doan, P. E., Hoffman, B. M., and Que, L., Jr. (2002) *J. Am. Chem. Soc. 124*, 2595−2603.
27. DeRose, V. J., Liu, K. E., Lippard, S. J., and Hoffman, B. M. (1996) *J. Am. Chem. Soc. 118*, 121−134.
28. DeRose, V. J., Liu, K. E., Kurtz, D. M., Hoffman, B. M., and Lippard, S. J. (1993) *J. Am. Chem. Soc. 115*, 6440−6441.
29. Werst, M. M., Davoust, C. E., and Hoffman, B. M. (1991) *J. Am. Chem. Soc. 113*, 1533−1538.
30. Davoust, C. E., Doan, P. E., and Hoffman, B. M. (1996) *J. Magn. Reson. 119*, 38−44.
31. Mims, W. B. (1965) *Proc. R. Soc. London A 283*, 452−457.
32. Gemperle, C., and Schweiger, A. (1991) *Chem. Rev. 91*, 1481−1505.
33. Doan, P. E., and Hoffman, B. M. (1997) *Chem. Phys. Lett. 269*, 208−214.
34. Davies, E. R. (1974) *Phys. Lett. A 47A*, 1−2.
35. Fan, C. L., Doan, P. E., Davoust, C. E., and Hoffman, B. M. (1992) *J. Magn. Reson. 98*, 62−72.
36. Hoffman, B. M., DeRose, V. J., Doan, P. E., Gurbiel, R. J., Houseman, A. L. P., and Telser, J. (1993) *Biol. Magn. Res. 13*, 151−218.
37. DeRose, V. J., and Hoffman, B. M. (1995) *Methods Enzymol. 246*, 554−589.
38. Davydov, R., Kuprin, S., Graslund, A., and Ehrenberg, A. (1994) *J. Am. Chem. Soc. 116*, 11120−11128.
39. Whittington, D. A., and Lippard, S. J. (2001) *J. Am. Chem. Soc. 123*, 827−838.
40. Willems, J.-P., Lee, H.-I., Burdi, D., Doan, P. E., Stubbe, J., and Hoffman, B. M. (1997) *J. Am. Chem. Soc. 119*, 9816−9824.
41. Epel, B., Poppl, A., Manikandan, P., Vega, S., and Goldfarb, D. (2001) *J. Magn. Reson. 148*, 388−397.
42. Gurbiel, R. J., Ohnishi, T., Robertson, D. E., Daldal, F., and Hoffman, B. M. (1991) *Biochemistry 30*, 11579−11584.
43. Davydov, R. M., Smieja, J., Dikanov, S. A., Zang, Y., Que, L., Jr., and Bowman, M. K. (1999) *J. Biol. Inorg. Chem. 4*, 292−301.
44. Davydov, R. M., Menage, S., Fontecave, M., Graslund, A., and Ehrenberg, A. (1997) *J. Biol. Inorg. Chem. 2*, 242−255.
45. Bossek, U., Hummel, H., Weyhermuller, T., Bill, E., and Wieghardt, K. (1995) *Angew. Chem., Int. Ed. Engl. 34*, 2642−2645.
46. Payne, S. C., and Hagen, K. S. (2000) *J. Am. Chem. Soc. 122*, 6399−6410.
47. Sage, J. T., Xia, Y.-M., Debrunner, P. G., Keough, D. T., de Jersey, J., and Zerner, B. (1989) *J. Am. Chem. Soc. 111*, 7239−7247.
48. Kurtz, D. M., Jr. (1990) *Chem. Rev. 90*, 585−606.
49. Davydov, R., Makris, T. M., Kofman, V., Werst, D. E., Sligar, S. G., and Hoffman, B. M. (2001) *J. Am. Chem. Soc. 123*, 1403−1415.
50. Davydov, R., Kofman, V., Fujii, H., Yoshida, T., Ikeda-Saito, M., and Hoffman, B. M. (2002) *J. Am. Chem. Soc. 124*, 1798−1808.

BI0300027